

Single molecule fluorescence in rectangular nano-apertures

Jérôme Wenger, Pierre-François Lenne, Evgueni Popov and Hervé Rigneault

*Institut Fresnel, Domaine Universitaire de Saint Jérôme, Université Paul Cézanne
Aix-Marseille III, CNRS UMR6133, 13397 Marseille Cedex 20, France*

lenne@fresnel.fr

herve.rigneault@fresnel.fr

José Dintinger and Thomas W. Ebbesen

ISIS, Université Louis Pasteur, CNRS UMR 7006, 8 allée G. Monge, 67000 Strasbourg, France

Abstract: Fluorescence Correlation Spectroscopy is used to investigate fluorescent molecules in solution diffusing in subwavelength rectangular apertures milled in Aluminium films. This rectangular shape allows to switch between a propagating and an evanescent excitation field within the aperture, leading to a significant tunability of the observation volume. Due to the vicinity of the metal surface, the fluorophore's molecular lifetime inside the aperture appears to be dramatically reduced whatever the excitation field is set to. However, for a properly tailored evanescent excitation field within the nanoaperture, the detected fluorescence rate per molecule is significantly enhanced as compared to open solution. This suggests that the observed molecular fluorescence enhancement is mainly due to the excitation near field within the subwavelength aperture.

© 2005 Optical Society of America

OCIS codes: (050.1220) Apertures; (180.2520) Fluorescence microscopy; (240.6680) Surface plasmons

References and links

1. N. Hayasawa, Y. Inouye and S. Kawata, "Evanescent field excitation and measurement of dye fluorescence in a metallic probe near-field scanning optical microscope," *J Microsc* **194**, 472-476 (1999).
2. J. Azoulay, A. Débarre, A. Richard and P. Tchério, "Field enhancement and apertureless near-field optical spectroscopy of single molecules," *J Microsc* **194**, 486-490 (1999).
3. H.F. Hamann, A. Gallagher and D.J. Nesbitt, "Near-field fluorescence imaging by localized field enhancement near a sharp probe tip," *Appl. Phys. Lett.* **76**, 1953-1957 (2000).
4. E.J. Sánchez, L. Novotny and X.S. Xie, "Near-Field Fluorescence Microscopy Based on Two-Photon Excitation with Metal Tips," *Phys. Rev. Lett.* **82**, 4014-4017 (1999).
5. B. Knoll and F. Keilmann, "Near-field probing of vibrational absorption for chemical microscopy," *Nature* **399**, 134-136 (1999).
6. Y. Inouye, N. Hayasawa, K. Hayashi, Z. Sekkat and S. Kawata, "Near-field scanning optical microscope using a metallized cantilever tip for nanospectroscopy," *Proc SPIE Int. Soc. Eng.* **3791**, 40-48 (1999).
7. T. Ichimura, N. Hayasawa, M. Hashimoto, Y. Inouye and S. Kawata, "Tip-Enhanced Coherent Anti-Stokes Raman Scattering for Vibrational Nanoimaging," *Phys. Rev. Lett.* **92**, 220801-220804 (2004).
8. *Near-Field Optics and Surface Plasmon Polaritons*, edited by S. Kawata (Springer, Berlin, 2001).
9. S. Nie and S.R. Emory, "Probing single molecule and single nanoparticles by surface enhanced Raman scattering," *Science* **275**, 1102-1106 (1997).
10. K. Kneipp, H. Kneipp, I. Itzkan, R.R. Dasari and M.S. Feld, "Surface-enhanced non-linear Raman scattering at the single-molecule level," *Chem. Phys.* **247**, 155-162 (1999).

11. H. Yokota, K. Saito and T. Yanagida, "Single Molecule Imaging of Fluorescently Labeled Proteins on Metal by Surface Plasmons in Aqueous Solution," *Phys. Rev. Lett.* **80**, 4606-4609 (1998).
12. F.D. Stefani, K. Vasilev, N. Bocchio, N. Stoyanova and M. Kreiter, "Surface-Plasmon-Mediated Single-Molecule Fluorescence Through a Thin Metallic Film," *Phys. Rev. Lett.* **94**, 023005-1-4 (2005).
13. M.J. Levene, J. Korfach, S.W. Turner, M. Foquet, H.G. Craighead and W.W. Webb, "Zero-mode waveguides for single-molecule analysis at high concentrations," *Science* **299**, 682-686 (2003).
14. K.T. Samiec, M. Foquet, L. Guo, E.C. Cox and H.G. Craighead, " λ repressor oligomerization kinetics at high concentrations using fluorescence correlation spectroscopy in zero-mode waveguides," *Biophys. J.* **88**, 2145-2153 (2005).
15. H. Rigneault, J. Capoulade, J. Dintinger, J. Wenger, N. Bonod, E. Popov, T. W. Ebbesen, and P-F. Lenne, "Enhancement of single-molecule fluorescence detection in subwavelength apertures," accepted for publication in *Phys. Rev. Lett.* (2005).
16. T. W. Ebbesen, H. J. Lezec, H. F. Ghaemi, et al., "Extraordinary optical transmission through subwavelength hole arrays," *Nature* **391**, 667-669 (1998).
17. H. J. Lezec, A. Degiron, E. Devaux, et al., "Beaming light from a subwavelength aperture," *Science* **297**, 820-822 (2002).
18. A. Degiron, H. J. Lezec, N. Yamamoto, et al., "Optical transmission properties of a single subwavelength aperture in a real metal," *Opt. Commun.* **239**, 61-66 (2004).
19. E. Popov, N. Bonod, M. Nenièvre, H. Rigneault, P-F. Lenne and P. Chaumet, "Surface plasmon excitation on a single subwavelength hole in a metallic sheet," *Appl. Opt.* **44**, 2332-2337 (2005).
20. A. R. Zakharian, M. Mansuripur, and J. V. Moloney, "Transmission of light through small elliptical apertures," *Opt. Express* **12**, 2631-2648 (2004).
21. L. Yin, V. K. Vlasko-Vlasov, A. Rydh, et al., "Surface plasmons at single nanoholes in Au films," *Appl. Phys. Lett.* **85**, 467-469 (2004).
22. E. M. Purcell, "Spontaneous emission probabilities at radio frequencies," *Phys. Rev.* **69**, 681 (1946).
23. H. Gersen, M. F. Garcia-Parajo, L. Novotny, et al., "Influencing the Angular Emission of a Single Molecule," *Phys. Rev. Lett.* **85**, 5312-5315 (2000).
24. D. Magde, E. Elson and W.W. Webb, "Thermodynamic Fluctuations in a Reacting System Measurement by Fluorescence Correlation Spectroscopy," *Phys. Rev. Lett.* **29**, 705-708 (1972).
25. E. Elson and D. Magde, "Fluorescence correlation spectroscopy. II. An experimental realization," *Biopolymers* **13**, 29-61 (1974).
26. W.P. Ambrose, P.M. Goodwin, J.C. Martin et al., "Alterations of Single Molecule Fluorescence Lifetimes in Near-Field Optical Microscopy," *Science* **265**, 364-366 (1994).
27. R.X. Brian, R.C. Dunn and X.S. Xie, "Single Molecule Emission Characteristics in Near-Field Microscopy," *Phys. Rev. Lett.* **75**, 4772-4775 (1995).
28. *Single-Molecule Detection in Solution - Methods and Applications*, edited by C. Zander, J. Enderlein and R.A. Keller (VCH-Wiley, Berlin/New York, 2002).

1. Introduction

Metallic devices at the nanometer scale have stimulated a broad range of interests in nanophotonics and near-field microscopy. For instance, sharp apertureless metal tips have been used to enhance the signal-to-noise ratio and the spatial resolution in a wide range of experiments: fluorescence [1, 2, 3], two-photon-excited fluorescence [4], infrared absorption [5], Raman scattering [6] and coherent anti-Stokes Raman scattering [7]. At the vicinity of the metallic tip end, the excitation of the local mode of the surface plasmon polaritons and the singular behavior of the electromagnetic field (lightning-rod effect) give rise to an enhancement of the electric field [8]. Experiments have also shown that the fluorescence of single molecules in the vicinity of a thin metallic film may appear enhanced up to a factor of 12 when detected through the metallic film [11, 12].

The use of isolated nanometric circular holes milled in metallic films has offered new applications for single molecule analysis in a highly concentrated solution (with concentrations up to the millimolar), studied using standard fluorescence correlation spectroscopy techniques [13, 14, 15]. In these experiments, tiny subwavelength apertures were shown to act as small reaction chambers containing in average a few molecules. This allows to reduce the observation volume by 3 to 6 orders of magnitude, from one femtoliter (obtained by a standard confocal microscope) to the attoliter or zeptoliter range (10^{-18} or 10^{-21} l). Thus, in turn, techniques such

as fluorescence correlation spectroscopy which only work while observing a small number of molecules are readily applicable to significantly higher molecular concentrations. This point is of particular importance while studying biologically relevant enzyme kinetics which generally require concentrations in the micro- to millimolar range [14, 13].

Using isolated circular apertures of diameters between 110 and 420 nm milled in Al films, we reported a striking enhancement of the molecular fluorescence as compared to open solution (with a significant increase up to 6.5 fold), together with a strong reduction of the molecular lifetime within the aperture [15]. This findings appear closely linked with the existence of localized surface plasmon (LSP) modes that have been observed at the entrance of the subwavelength apertures [18].

If these studies validate the potential of single nanometric apertures milled in metal films to reduce the observation volume and increase the detected fluorescence rate per molecule, the concepts involved in the fluorescence enhancement still remain unclear as many different effects may play a role : (i) the local excitation intensity I_{ex} is expected to be enhanced due to charge accumulation at the edges of the nanohole excited by the linearly-polarized incoming field [19, 20, 21], (ii) the lifetime reduction in the apertures postpones saturation effects [22] and allows for an increase in the fluorescence rate, (iii) the radiation pattern can be affected by the metallic subwavelength aperture boundary conditions [23], thus leading to a higher collection efficiency. Besides, one has to take into account the role played by the LSP modes in the effects (i)-(iii) [18].

In this letter, we bring new insights on the mechanisms leading to an enhancement of the detected fluorescence while using metallic nanoapertures. This is achieved by studying isolated rectangular nanostructures milled in metallic films with various aspect ratios. This particular aperture shape allows to switch between the activation of two distinct modes by changing the angle θ between the linearly-polarized incoming electric field and the longitudinal direction of the hole (see Fig. 1). Since the waveguide's cut-off wavelength is different for each axis, the penetration depth of the excitation light within the aperture can thus be significantly tuned, offering new possibilities to tailor the observation volume. Surprisingly, we also show that a high transmission of the excitation field does not yield any fluorescence enhancement whereas an evanescent coupling of the pump field induces a significant increase in the detected count rate per molecule. These results suggest that the observed molecular fluorescence enhancement is mainly related to the near field intensity within the subwavelength aperture.

This manuscript is organized as follows : we first describe our experimental apparatus and characterize the samples in terms of their transmission versus the incoming polarization (section 2). Section 3 then focuses on the molecular characteristics within the nanohole studied thanks to fluorescence correlation spectroscopy.

2. Materials

2.1. Experimental setup

Optically thick aluminium films (thickness 250 nm) were coated on conventional microscope slips (thickness 150 μm) by thermal evaporation. Rectangular subwavelength apertures were then milled by focused ion beam (FEI Strata DB235) using Ga⁺ ions exhibiting a 5 nm nominal beam diameter. Figure 1 shows the SEM micrograph image of such an aperture. Depending on the desired aspect ratio, the long edge may vary between 190 to 565 nm, while the small edge measures between 90 to 250 nm.

The molecular fluorescence characteristics within the nanostructure are analyzed here thanks to the technique of fluorescence correlation spectroscopy (FCS) [24] : the fluorescence photo-count signal $n(t)$ is recorded and its temporal autocorrelation is computed. This is quantified by

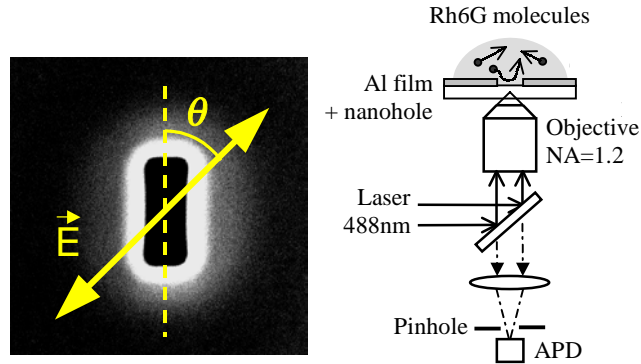


Fig. 1. Left : Scanning electron microscope image of an isolated $340 \times 115 \text{ nm}^2$ subwavelength aperture milled in an Al film coated on a microscope slip. Right : schematic view of the optical setup for fluorescence correlation spectroscopy (APD : avalanche photodiode).

the fluctuation autocorrelation function:

$$g^{(2)}(\tau) = \frac{\langle n(t)n(t+\tau) \rangle}{\langle n(t) \rangle^2}, \quad (1)$$

where $\langle \cdot \rangle$ stands for an ensemble averaging. This procedure allows to determine both the average number of molecules present in the observation volume and the average number of photons detected per molecule and per second. Let us emphasize that because the molecules are permanently diffusing in and out of the observation volume, our experiments are not sensitive to the molecular dipole orientations nor to each molecule trajectory individually, but provide knowledge on the average behavior of the molecular fluorescence and diffusion.

Fluorescence correlation spectroscopy experiments were performed in a custom setup based on an inverted microscope (Zeiss Axiovert 200) with an NA=1.2 objective lens (Zeiss C-Apochromat). Nanopositioning of the aperture was possible thanks to a multi-axis piezo stage (Physik Instrumente P527). Intensity autocorrelations were recorded by a hardware correlator (ALV 6000). We used as fluorescent probes Rhodamine 6G molecules (Rh6G) with an excitation wavelength of 488 nm provided by an argon ion laser (see Fig. 1). Tight focusing conditions were used to illuminate a single subwavelength aperture with a beam waist of 250 nm, (calibrated from FCS experiments carried out on Rh6G in solution). This setup provides an observation volume V_{eff} without a nanoaperture of 750 attoliters. The laser polarization was set linear and was rotated using a zero-order half-waveplate.

2.2. Optical transmission properties of rectangular nanoholes

The transmission of the monochromatic 488 nm excitation field through a rectangular nanohole is presented on Fig. 2 while changing the angle θ between the linearly polarized electric field and the longitudinal direction. For the rectangular hole with the greatest aspect ratio length / width, the transmission follows a standard \cos^2 law, with a transmission almost null at $\theta = 0^\circ$ (extinction better than 1:60). This clearly indicates that one switches from a propagating mode when $\theta = \pm 90^\circ$ to an evanescent mode when $\theta = 0^\circ$. These observations stand in well agreement with the propagation theory of modes through rectangular metallic waveguides, if one recalls that the cut-off wavelength for propagating TE modes polarized along one axis of a rectangular waveguide (of perfectly conducting metal) is given by $2nd$ where n is the refractive index inside the hole and d is the total hole length perpendicular to the electric field

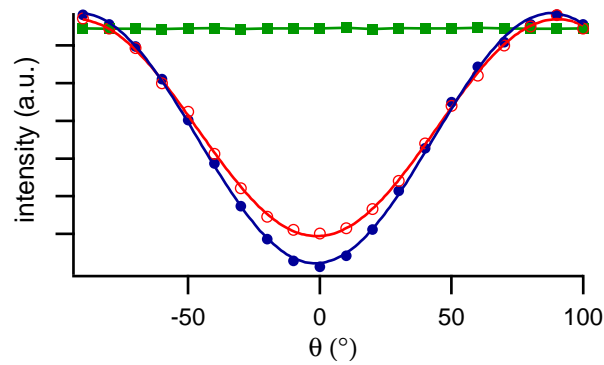


Fig. 2. Intensity transmission properties of an isolated rectangular $565 \times 105 \text{ nm}^2$ (blue filled circles), $380 \times 160 \text{ nm}^2$ (red empty circles), or squared $250 \times 250 \text{ nm}^2$ (green boxes) nanometric aperture measured at 488 nm while changing the incoming linear polarization direction θ .

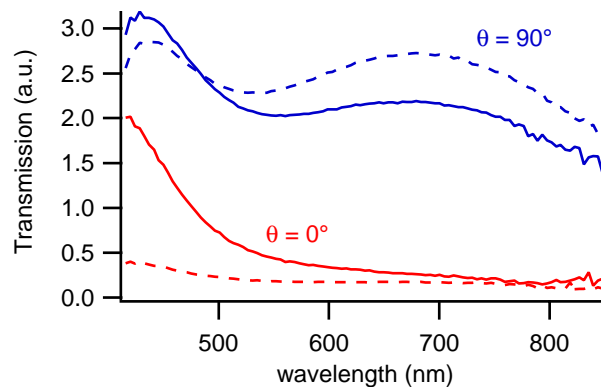


Fig. 3. Transmission spectrum of a $490 \times 105 \text{ nm}^2$ rectangular hole milled in an Al layer for different linear polarization direction θ of the excitation field, when a droplet of water is deposited over the aperture (solid curves), or when the metal surface is left dry (dashed curves).

polarization. Thus for $\theta = 0^\circ$ the cut-off wavelength is given by the minor axis of the hole and is much smaller than for the case corresponding to $\theta = 90^\circ$. As expected, the extinction ratio of the transmitted light versus θ increased while working with nanoholes of higher aspect ratios, as shown on Fig. 2. On the contrary, the transmission versus θ remains constant for a squared nanometric hole. This can be seen as a direct consequence of Maxwell's equations linearity by expressing an arbitrary polarization θ as a sum of two orthogonal polarizations along the hole axis.

To gain insight about possible resonances at some specific wavelengths, we recorded the transmission spectrum of the rectangular apertures for various linear polarizations. As shown on Fig. 3, the transmission remains almost constant over the $500\text{-}700 \text{ nm}$ window when a droplet of water is deposited over the metal surface. The discrepancy between this result and the spectral curves presented in [18] may be explained by the fact that we are working with aluminium films instead of silver and are studying holes in films on substrate: here the adjacent dielectric media have different refractive indexes and therefore the energies of the LSP modes are different. This mismatch in frequency decreases the tunnelling probability through the hole and thus the

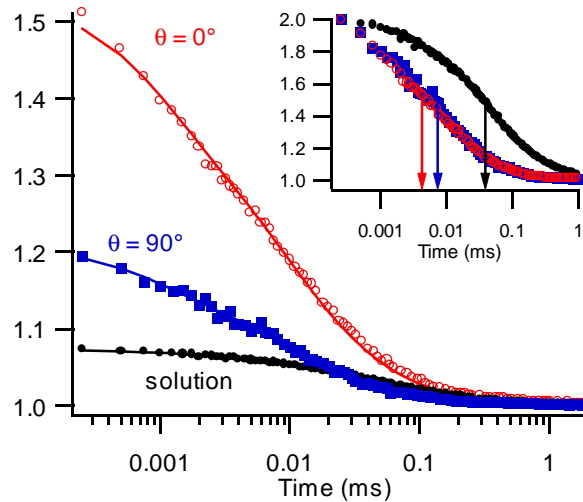


Fig. 4. Fluorescence autocorrelation functions in open solution (black dots) and in a $565 \times 105 \text{ nm}^2$ hole for $\theta = 0^\circ$ (red empty circles) and $\theta = 90^\circ$ (blue filled squares) for an excitation power of $300 \mu\text{W}$. The molecular concentration for the experiment in open solution was set to 20 nM , while it was taken to 300 nM within the aperture. The solid lines originate from numerical fits assuming a 3D diffusion. For the $565 \times 105 \text{ nm}^2$ aperture and $\theta = 0^\circ$, one gets $N = 0.3$, $n_T = 0.35$, count rate per molecule = 50 kHz , while for $\theta = 90^\circ$, $N = 2.4$, $n_T = 0.35$, count rate per molecule = 18 kHz (the background mean intensity was $\langle b \rangle = 30 \text{ kHz}$). The inset shows the same traces normalized to unity (arrows indicate the time at half-maximum).

transmission peaks due to the LSPs are no longer easily detectable [18].

3. Single molecule fluorescence in subwavelength apertures

3.1. Observation volume tunability

Let us now study the diffusion dynamics of fluorescent rhodamine 6G molecules within the nanoholes. The mean number of molecules N present in the observation volume V_{eff} is obtained from the intensity autocorrelation function value at the origin ($\tau = 0$):

$$g^{(2)}(\tau) = 1 + \frac{1 + n_T(1 + \exp(-\tau/\tau_T))}{N} \left(1 - \frac{\langle b \rangle}{\langle i \rangle}\right)^2 \frac{1}{(1 + \tau/\tau_d)\sqrt{1 + s^2\tau/\tau_d}} \quad (2)$$

where n_T is the triplet amplitude, τ_T the triplet time, $\langle i \rangle$ the mean intensity, $\langle b \rangle$ the mean background, τ_d the diffusion time and s the ratio of transversal to axial dimensions of the observation volume. This expression assumes a 3D Brownian diffusion. However, let us point out that at $\tau = 0$ this formula is independent of the shape of the excitation field and the type of the diffusion statistics [25]. The triplet amplitude n_T is related to the fraction F of molecules in the triplet state by $F = n_T/(1 + n_T)$. For each experimental run, the triplet amplitude n_T was fitted to the experimental autocorrelation functions (assuming a 3D diffusion, see Fig. 4). For instance, n_T was found in the range $n_T = 0.35 \pm 0.15$ for the various aperture sizes and an excitation power of $300 \mu\text{W}$. Finally, special care was taken in the experiments to accurately calibrate the background noise within the apertures. We point out that the conditions leading to photobleaching were avoided in the experiments reported here, as the average number of Rh6G molecules and diffusion time remained constant when we increased the excitation power.

Table 1. Experimental results when θ is switched from 90° to 0° .

Dimensions (nm ²) ^a	Aspect ratio	V_{eff} reduction ^b	Fluorescence enhancement ^c
190 x 190	1 : 1	1	3.2
280 x 140	1 : 2.0	2.5	3.1
340 x 115	1 : 3.0	3.2	3.2
420 x 90	1 : 4.7	6.0	3.2
250 x 250	1 : 1	1	2.0
345 x 175	1 : 2.0	2.1	2.1
380 x 160	1 : 2.4	2.7	2.3
565 x 105	1 : 5.4	8.0	2.5

^a Each group of four apertures corresponds to a constant surface, respectively 0.04 and 0.06 μm^2 .

^b The observation volume V_{eff} reduction while switching the polarization from $\theta = 90^\circ$ to $\theta = 0^\circ$ is computed from the ratio $N_{\theta=90}/N_{\theta=0}$ of the mean number of molecules detected for each polarization.

^c The fluorescence enhancement is given by the ratio of the photonic count rate per molecule per second in the nanohole as compared to open solution, when the polarization is set to $\theta = 0^\circ$, corresponding to an evanescent coupling of the pump field (excitation power : 300 μW). When $\theta = 90^\circ$, no fluorescence enhancement could be detected.

Table 1 presents the observation volume alteration when changing the excitation polarization from $\theta = 90^\circ$ to $\theta = 0^\circ$. As expected from the transmission properties of the rectangular nanoholes, when $\theta = \pm 90^\circ$ the pump field propagates maximally through the hole and the number of detected molecules is then maximal. When the polarization is turned to $\theta = 0^\circ$ the pump couples evanescently inside the hole and the number of detected molecules is significantly reduced. Thus by changing the excitation field, one may easily tailor the observation volume V_{eff} and reduce it by a factor as large as 8 for a 565 x 105 nm² aperture.

The volume reduction is linked with a reduction of the diffusion time across V_{eff} as illustrated by the (normalized) autocorrelation functions presented in Fig. 4, which are recorded into a 565 x 105 nm² aperture. We found that this diffusion time reduction is qualitatively consistent with the volume awaited from the penetration depth of an evanescent wave through a nanohole (about 90 nm for a 105 nm aperture and a wavelength of 488 nm). However, performing a complete theoretical description of the volume reduction is a challenging task, because V_{eff} depends not only on the pump intensity profile within the hole, but also on the fluorophore's coupling efficiency and its quantum yield. Such an analysis is beyond the scope of this paper.

3.2. Fluorescence enhancement

Besides the reduction of V_{eff} , we investigated the molecular fluorescence process inside the nanoapertures as compared to open solution. Relevant information is given by the average detected count rate per molecule η within the aperture, which is readily obtained by dividing the total average number of photocounts per second by the average number of molecules N computed from $g^{(2)}(0)$. The last column of table 1 presents the enhancement of η as compared to its value in open solution for an excitation power of 300 μW and $\theta = 0^\circ$ (evanescent coupling of the pump field). A significant enhancement is observed for small holes surfaces, which is consistent with the observations reported for circular holes [15]. For these experiments, the excitation power was set so that the fluorescence remained in the linear regime for experiments

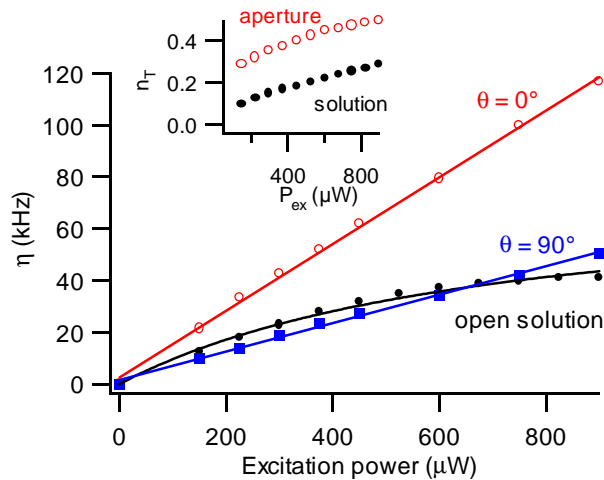


Fig. 5. Detected count rate per molecule per second η versus the incident excitation power P_{ex} in a $565 \times 105 \text{ nm}^2$ aperture and in open solution. The inset displays the influence of the excitation power on the triplet amplitude n_T (obtained from numerical fits and used in our calculations).

carried in the nanoaperture or in open solution. However, when $\theta = 90^\circ$, no fluorescence enhancement could be detected for rectangular apertures (except squared holes), as the photonic count rate per molecule η remained almost the same as in open solution. In other words, as soon as the field wavelength is shorter than the waveguide's cut-off wavelength (propagating field), no fluorescence enhancement is observed at all. Thus a high transmission of the pump field is not correlated with an increase in the detected fluorescence rate.

This result may look surprising if one thinks about the excitation of localized surface plasmon (LSP) modes which play an important role into the near field intensity within and around the nanoaperture. In [18], it was shown that the LSP modes are localized on the edges perpendicular to the electric field. Thus changing θ from 0° to 90° allows to excite either the transverse or longitudinal edges. Naively, one would expect that the longitudinal mode excitation ($\theta = 90^\circ$) leads to a significantly higher fluorescence enhancement, due to the much larger edges size involved. However, this statement appears not to be verified experimentally, as the longitudinal mode excitation ($\theta = 90^\circ$) leads to a high transmission of the pump field but to no fluorescence enhancement at all, whereas the excitation of the transverse mode with small edges ($\theta = 0^\circ$) yields a significant fluorescence enhancement. At this point, we can conclude that the near field excitation intensity is deeply involved into the observed molecular fluorescence enhancement.

Some better understandings is provided by the evolution of the detected count rate per molecule η versus the excitation power P_{ex} in a $565 \times 105 \text{ nm}^2$ aperture and in open solution (see Fig. 5, which appears as our main experimental result). In the linear regime ($P_{ex} < 0.4 \text{ mW}$) and for $\theta = 0^\circ$, η was enhanced up to ~ 2.5 times as compared to open solution. For $\theta = 90^\circ$, the detected count rate per molecule in the aperture almost follows the calibration obtained for the open solution, showing no enhancement at all. Let us emphasize that no photobleaching processes were involved in these experiments, as we observed that the diffusion time and number of molecules remained constant for our whole range of excitation powers. Besides, since Rh6G is a high quantum efficiency dye, the triplet amplitude n_T remains quite small while increasing the excitation power. The inset of Fig. 5 displays the evolution of n_T versus the excitation power, obtained from numerical fits on our experimental autocorrelation functions.

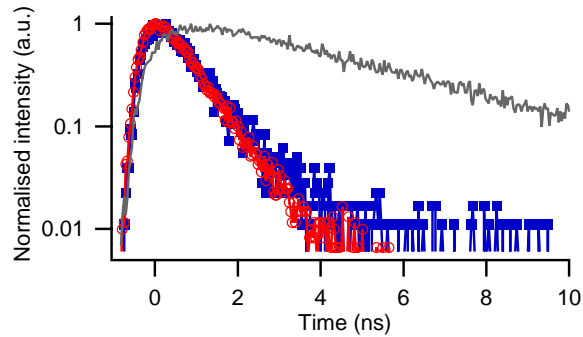


Fig. 6. Fluorescence decay curves in open solution (solid gray) and into a $565 \times 105 \text{ nm}^2$ nanohole for $\theta = 0^\circ$ (red empty circles) and $\theta = 90^\circ$ (blue filled squares).

A major point to notice on Fig. 5 is that the fluorescence linear regime persists in nanoapertures up to $P_{ex} \sim 0.9 \text{ mW}$ for both polarizations, whereas η saturates to $\sim 40 \text{ kHz}$ when $P_{ex} > 0.4 \text{ mW}$ for Rh6G molecules in open solution. Unfortunately, the excitation power could not be increased over 1 mW due to sample damages occurring at high pump intensities, and thus no saturation of η could be detected within the nanoapertures. This curve illustrates a major feature of the use of nanoholes : for a properly tailored excitation field in the subwavelength aperture, one can detect count rates greater than one hundred thousands photons per second and per molecule, whereas for a single molecule in open solution the detected fluorescence never exceeds a few tens of kilocounts per second.

To understand this delay in the saturation of the fluorescence process, we investigated the molecular fluorescence lifetime within the nanoholes versus the incoming polarization. Figure 6 shows the Rh6G fluorescence radiative decay curves in open solution and in a $565 \times 105 \text{ nm}^2$ nanoaperture when the excitation field polarization is changed from $\theta = 0^\circ$ to $\theta = 90^\circ$. These curves were recorded by a time to amplitude converter (TimeHarp-PicoQuant) following a 4 MHz pulse train provided by a linearly polarised picosecond Ti:Saph laser tuned at 800 nm (performing two-photon excitation). Inside the nanoaperture, a major reduction of the molecular lifetime is observed from 3.7 ns in open solution down to our apparatus response time (0.9 ns), independently of the incoming polarization direction θ . This result clearly indicates that the molecular energy levels branching ratios are affected for molecules located in the nanoapertures, allowing for a delay of the fluorescence saturation. Moreover, as far as our measurements could reveal, the fluorescence lifetime appears independent of the excitation field mode, and mainly dictated by the fluorophore's metallic environment. This point is confirmed by previously reported investigations [26, 27]. Importantly, let us point out that the molecular lifetime is significantly reduced for $\theta = 90^\circ$ without yielding any fluorescence enhancement (for excitation powers in the linear regime). Thus an alteration of the molecular energy levels branching ratios can not solely account for the reported fluorescence increase. Other parameters have to be considered, at most the local excitation intensity I_{ex} , as already suggested in the previous section.

When dealing with excitation powers well below the saturation intensity of the absorption-emission cycle, the fluorescence rate η appears directly proportional to the excitation intensity I_{ex} and to the collection efficiency [28]. A complete theoretical description of the fluorescence enhancement process would require the computation of the local collection efficiency function (including molecular absorption) and the local excitation intensity for a real metal, which is beyond the scope of this paper. However, one may gain some insight by noticing that the curves of η for $\theta = 0^\circ$ and $\theta = 90^\circ$ on Fig. 5 bear different slopes, and that their ratio remains almost

constant over the whole excitation power range. Considering that the environment of the diffusing fluorophore is almost the same for $\theta = 0^\circ$ and $\theta = 90^\circ$, one may undertake the assumption that the collection efficiency is identical for both polarizations. Consequently, the ratio of the fluorescence rates per molecule $\eta(\theta = 0^\circ) / \eta(\theta = 90^\circ)$ is a direct witness of the local excitation intensities ratio $I_{ex}(\theta = 0^\circ) / I_{ex}(\theta = 90^\circ)$, which is in others words the ratio of the local intensities for an evanescent and a propagating field within the aperture (about 2.4 in the case of the nanohole of Fig. 5). We can conclude that the observed fluorescence enhancement could thus be explained by an increase in the local excitation intensity due to the evanescent coupling of the pump field within the aperture. This local excitation enhancement may be linked to some efficient excitation of surface plasmon modes localized close to the edges of the nanoaperture, as numerically demonstrated for circular nanoholes [19, 15]. Of course, other effects may come into play to fully explain the detected fluorescence enhancement, but they seem to be of minor importance in our observations. For instance, the study of circular nanoholes [15] demonstrated that an alteration of the radiation pattern cannot completely account for the observed enhancement.

4. Conclusion

By assessing the average properties of single molecules, fluorescence correlation spectroscopy proves to be a valuable tool to characterize the near-field optical properties of isolated nanostructures. We have shown that by using a rectangular nanoaperture milled in a metal film together with a linearly polarised excitation field, one may switch from a propagating to an evanescent optical mode within the aperture. This leads to significant tailoring possibilities of the observation volume and a further volume reduction for the evanescent excitation field.

Looking at the emission process inside the aperture, the metallic nanostructure allows on one hand to delay the saturation of the fluorescence process, while on the other hand, the detected count rate per molecule can be significantly enhanced, depending on the excitation field coupling within the nanoaperture. We show that a high transmission of the excitation field does not yield any fluorescence enhancement, whereas an evanescent excitation can be used to induce a significant increase in the detected count rate per molecule. Altogether, these results suggest that the observed molecular fluorescence enhancement in subwavelength apertures results mainly from an increase of the near field intensity within the aperture and that lifetime reduction and radiation pattern alteration play a minor role.

Acknowledgments

The authors wish to acknowledge the support of the "ACI Nanosciences" of the French Research Ministry.